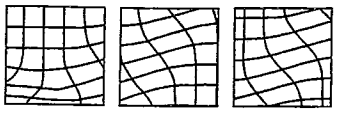

V encontro nacional de **mecânica** computacional
Universidade do Minho - Guimarães - 20 a 22 de Outubro de 1997

THE PLANE CONTRACTION FLOW OF UPPER CONVECTED MAXWELL FLUIDS CALCULATED BY A FINITE-VOLUME COLOCATED-MESH METHOD

P. J. Oliveira[1] and F. T. Pinho[2]

ABSTRACT

The prediction of real viscoelastic flows requires computational methods able to deal with complex boundaries and rheological models, a task within the reach of present day finite-volume techniques. A new finite-volume based algorithm was developed for calculations of the flow of Upper Convected Maxwell (UCM) fluids in a general non-orthogonal colocated grid, and was used to predict the flow in a planar 4:1 sudden contraction. All terms of the equations were kept and the discretization and interpolation techniques were either first or second order accurate. Pressure-velocity-stress coupling was ensured through a new interpolation technique for the momentum equation, which was developed to include the stress tensor.

Calculations in the 4:1 contraction flow of Newtonian and UCM fluids were carried out for Reynolds numbers of 0.01 and 10 and Deborah numbers up to 10.0, and the results compared favourably with those available in the literature. The tested range of Deborah numbers was somewaht extended to that found in the literature for finite-element methods. Profiles of all calculated quantities were smooth and grid independent, except for the stresses in the vicinity of the re-entrant corner where the maximum values depended on the grid size because, as is well known, they tend to infinity even for the Newtonian case. All the components of the stress tensor increased with elasticity in the re-entrant corner, especially the axial normal stress.

1. INTRODUCTION

Methods based on finite-volumes can be advantageous for the calculation of fluid flows in terms of computer space, time requirements and numerical stability, in comparison to finite-element methods, but in spite of these advantages they have not been used in the computation of non-Newtonian viscoelastic fluid flows for quite a long time.

[1] Departamento de Engenharia Electromecânica, Universidade da Beira Interior, Rua Marquês D'Ávila e Bolama, 6200 Covilhã, Portugal

[2] Departamento de Engenharia Mecânica e Gestão Industrial, Faculdade de Engenharia, Rua dos Bragas, 4099 Porto Codex, Portugal

Non-Newtonian fluids can exhibit complex flow patterns because of their highly non-linear behaviour, as is well documented in the visualisations of Boger and Walters (1993). One such example is the sudden contraction flow of viscoelastic fluids: the size and shape of the large vortex found upstream of the plane of the contraction strongly depends on the rheology of the fluid, especially on the elongational viscosity and elastic properties, contraction ratio and Reynolds number.

Early experimental work on this flow were the measurements of integral quantities of Boger and Ramamurthy (1970) and the flow visualisations of Walters and Webster (1982). Boger et al (1987) observed two vortices upstream of the sudden contraction plane with elastic fluids of constant viscometric viscosity: a large one in the salient corner, also found with Newtonian fluids but much weaker, and a smaller lip vortex near the re-entrant corner of the geometry. Both eddies interacted and grew with elasticity into a single large vortex, as the pressure drop across the contraction increased. Minor changes on surface edge quality dramatically changed the flow characteristics as found by Evans and Walters (1988). New flow patterns and flow transitions were identified in the detailed velocity measurements of Lawler et al (1986), whereas the role of the elongational viscosity and of the inertial forces on the vortex structure were investigated by Baloch et al (1994). Later, Quinzani et al (1994) have measured in detail the velocity and stress fields in a two-dimensional contraction for relatively low Deborah numbers.

The first numerical simulations of the contraction flow were not satisfactory because the constitutive models of Crochet and Pilate (1976) and Perera and Walters (1977) were too simple to predict real fluids. The adoption of more complex constitutive equations, such as the Upper Convective Maxwell (UCM) and Oldroyd B models, which have mathematical singularities (infinite elongational viscosity at rather low shear rates) lead to the first numerical problems. The calculations would not succeed for low values of the elasticity parameter, the Weissenberg (We) number (or Deborah number (De), for some authors). Various attempts at solving this problem with the finite-element technique by Rajagopalan et al (1990) and Webster (1986) were based on the decoupling of the elastic and viscous effects and a tighter control of these two properties to avoid and/or predict the change of the type of the rheological equation (hyperbolic/ elliptical) within the calculation domain.

Simultaneously, finite-volume methods progressed within the field of classical fluid mechanics (Ferziger and Peric, 1996). One of the first recent non-Newtonian finite-volume numerical investigations was that of Hu and Joseph (1990), who predicted successfully the flow of an UCM fluid around a cylinder at Reynolds and Weissenberg numbers of up to 10 using the SIMPLER algorithm with orthogonal staggered grids. The same methodology was adopted by Yoo and Na (1991), who predicted the flow in a sudden contraction, but without the inertia terms of the momentum equation. These are essential for calculations at moderate Reynolds number flows, but can result in convergence difficulties. In these and other simulations with the finite-volume technique (Sasmal, 1995), first order differencing schemes have been used in order to increase the maximum Weissenberg number for convergence.

There is clearly the need for developing a more general finite-volume methodology, which can be used in complex flow geometries and with complex fluids. Such program has been undertaken and is here reported. It relies on non-orthogonal coordinates together with colocated meshes, and an UCM model was initially adopted, but the algorithm is sufficiently general to facilitate the easy adoption of other constitutive equations.

The remaining of the paper presents the equations to be solved and an outline of the numerical method. This is followed by the presentation and discussion of the results of some calculations in a planar 4:1 sudden contraction.

2. GOVERNING EQUATIONS

The basic equations for three-dimensional, incompressible and isothermal laminar flow of an Upper Convected Maxwell fluid, hereafter referred to as the UCM fluid, are the continuity, the momentum and the rheological constitutive equations. Unless otherwise stated, the summation convention for repeated indices will apply.

The equations were discretized on a general computational finite-volume mesh composed of non-orthogonal six-faced cells. This entails transformation from an orthogonal coordinate system (x_1, x_2, x_3) into a general non-orthogonal coordinate system (ξ_1, ξ_2, ξ_3). These final equations are written in a strong conservation form so that all quantities are conserved in the final algebraic equations. The continuity equation is given by (1)

$$\frac{\partial}{\partial \xi_l}\left(\rho \beta_{lj} u_j\right) = 0 \tag{1}$$

$$\frac{\partial}{\partial t}\left(J\rho u_i\right) + \frac{\partial}{\partial \xi_l}\left(\rho \beta_{lj} u_j u_i\right) = -\beta_{li}\frac{\partial p}{\partial \xi_l} + \frac{\partial}{\partial \xi_l}\left(\beta_{lj}\tau_{ij}\right) + J\rho g_i \tag{2-a}$$

Since in the rhs of Eq. (2-a) a diffusion term, to be treated implicitly, does not appear explicitly, a modified momentum equation is used:

$$\frac{\partial}{\partial t}\left(J\rho u_i\right) + \frac{\partial}{\partial \xi_l}\left(\rho \beta_{lj} u_j u_i\right) - \frac{\partial}{\partial \xi_l}\left(\frac{\eta}{J}\beta_{lj}\beta_{lj}\frac{\partial u_i}{\partial \xi_l}\right) = -\beta_{li}\frac{\partial p}{\partial \xi_l} + \frac{\partial}{\partial \xi_l}\left(\beta_{lj}\tau_{ij}\right) + J\rho g_i - \frac{\partial}{\partial \xi_l}\left(\frac{\eta}{J}\beta_{lj}\beta_{lj}\frac{\partial u_i}{\partial \xi_l}\right) \quad \text{(no sum on l)} \tag{2-b}$$

in which all terms in the lhs are implicitly dealt with (incorporated into the coefficients) and those in the rhs are treated explicitly (incorporated into the source term).

The extra stress tensor τ_{ij} is defined by the UCM constitutive equation (3), where λ is the relaxation time, η the shear viscosity and the last term on the rhs is zero for incompressible fluids, but it is kept because it improves the convergence rate. In the transport equation (3), the terms which will be dealt with implicitly in the numerical procedure are written on the lhs.

$$J\tau_{ij} + \lambda\frac{\partial}{\partial t}\left(J\tau_{ij}\right) + \lambda\frac{\partial}{\partial \xi_l}\left(\beta_{lk}u_k\tau_{ij}\right) = \eta\left[\beta_{lj}\frac{\partial u_i}{\partial \xi_l} + \beta_{li}\frac{\partial u_j}{\partial \xi_l}\right] + \lambda\left[\left(\beta_{lk}\tau_{kj}\right)\frac{\partial u_i}{\partial \xi_l} + \left(\beta_{lk}\tau_{ki}\right)\frac{\partial u_j}{\partial \xi_l}\right] - \frac{2}{3}\eta\beta_{lk}\frac{\partial u_k}{\partial \xi_l}\delta_{ij} \tag{3}$$

3. NUMERICAL METHOD

In the finite-volume method the calculation domain is divided into cells and equations (1) - (3) are volume-integrated in each cell to ensure a conservative discretization. This is accomplished by applying Gauss' theorem, as explained in Oliveira et al (1997) and the discretization is performed with some differencing scheme applied to a universe of nodes constituted by those located at the centre of the cells and at the centre of their faces.

The discretised mass conservation equation, needed for the pressure, is

$$\sum_{\mathrm{f}}^{6}(-1)^{\mathrm{f}}F_{\mathrm{f}} = 0 \quad \text{with} \quad F_f = \sum_j\left(\rho B_{fj}\tilde{u}_j\right)_f \tag{4}$$

where the $(-1)^f$ is used to yield positive outgoing convective fluxes F_f and the face index varies from f = 1 to 6, for w, e, s, n, b and t, where compass notation is used. The procedure used to obtain the cell-face velocities $(\tilde{u}_i)_f$ is given later.

The nomenclature adopted here follows that of Oliveira et al (1997) and has the advantage of being readily generalised to non-structured grids in which there is no preferred direction. It is summarised in Figure 1, where a general cell P and its near neighbour cell F along direction $l=f$ across face f, are shown. The momentum equation was casted under the common linearised form u_i

$$a_P u_{i-P} = \sum a_F u_{i-F} + S_{u_i} + \frac{\rho V_P}{\delta t} u^o_{i-P} \tag{5-a}$$

where

$$a_P = \frac{\rho V_P}{\delta t} + a_0 + S_P \quad \text{and} \quad a_o \equiv \sum a_F \tag{5-b}$$

The neighbour coefficients (a_F) have convection (a_F^C) and diffusion (a_F^D) contributions. The diffusion term, added to the rhs of equation (2), leads to terms $a_F^D\, u_{i\text{-}F}$ that go to the general source S_{ui}, which is

$$S_{u_i} = S_{u_i - pressure} + S_{u_i - gravity} + S_{u_i - stress} + S^D_{u_i} + \sum a^C_{FF} u_{i-FF} \tag{6}$$

where the pressure, gravity and stress field sources are represented by $S_{ui\text{-}pressure}$, $S_{ui\text{-}gravity}$ and $S_{ui\text{-}stress}$. These are readily obtained from equation (2)

$$S_{u_i - pressure} = -\sum_{l=1}^{3} B^P_{li} [\Delta p]^P_l \tag{7-a}$$

$$S_{u_i - gravity} = \rho g_i V_P \tag{7-b}$$

$$S_{u_i - stress} = \sum_f (-1)^f \sum_j B^f_{fj} \tilde{\tau}^f_{ij} \tag{7-c}$$

$$S^D_{u_i} = -\sum_F a^D_F (u_{i-F} - u_{i-P}) \tag{7-d}$$

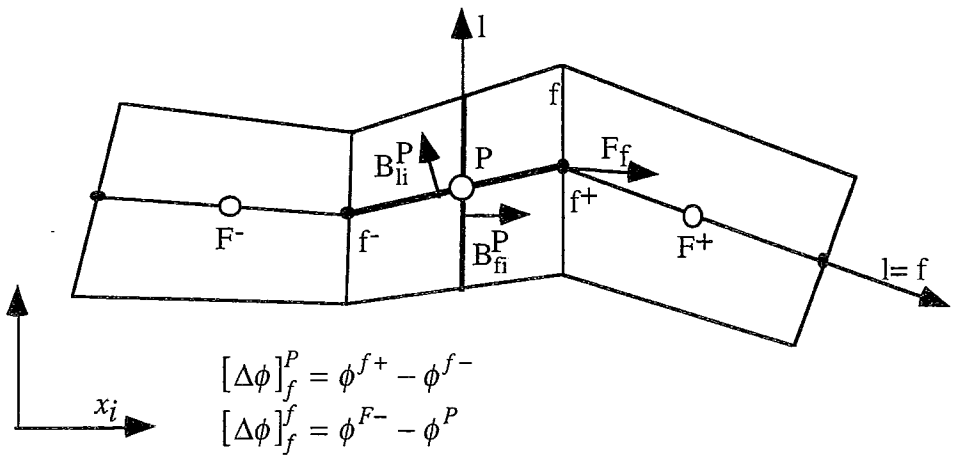

Fig. 1- Sketch of general cell and some nomenclature.

The last term on the rhs of equation (6) involves far-neighbour cells which originate from the use of a second-order accurate linear upwind scheme (LUDS) as the interpolation scheme for the convective terms. The central differencing (CDS) and upwind difference (UDS) schemes were also implemented in the program, in which case that term is absent from Eq. (6). The convective coefficients a_F^C are assembled from the face fluxes (4) following standard

expressions for the LUDS scheme given in Oliveira et al (1997). The diffusive coefficient, based on a central-difference integration, follows also the standard definition.

The central coefficient of the momentum equation, a_P in equation (5-b), contains S_P the linearized part of the average value of the source ($S^{ui} = S_{ui} - S_P u_i$) over the control volume. S_P considers those terms of the source which multiply $u_{i\text{-}P}$, and it also includes, for the LUDS scheme, the summation over the far-neighbour (ff) nodes ($\sum_{FF} a_{FF}$).

The discretized stress equation has a similar outlook to the momentum equation (2-b)

$$a_P^{\tau}\tau_{ij-P} = \sum a_F^{\tau}\tau_{ij-F} + S_{\tau_{ij}} + \frac{\lambda V_P}{\delta t}\tau_{ij-P}^{o} \tag{8}$$

except that there are no diffusive terms in the stress, i.e., the coefficients a_F^{τ} are composed by convective contributions only. The source term in (9) is evaluated at the centre of a cell, as

$$S_{\tau_{ij}} = \eta_P \sum_l^3 \left(B_{lj}^P [\Delta u_i]_l^P + B_{li}^P [\Delta u_j]_l^P \right) + \lambda_P \sum_l^3 \left(\left(\sum_k^3 B_{lk}^P \tau_{ik} \right) [\Delta u_j]_l^P + \left(\sum_k^3 B_{lk}^P \tau_{jk} \right) [\Delta u_i]_l^P \right) - \frac{2}{3}\eta_P \left(\sum_l^3 \sum_k^3 B_{lk}^P [\Delta u_k]_l^P \right) \delta_{ij} \tag{9}$$

Convective terms of the momentum and stress equations involve first derivatives of the quantities being convected, and thus lead to values of those quantities at the faces of the cells. These face values need to be computed from nodal values, a procedure which is based on an interpolation scheme.

The convective fluxes on the momentum equation were handled with a special interpolation scheme based on the scheme of Rhie and Chow (1982) (see Oliveira et al, 1997), enabling the calculation of ($\tilde{u}_{i-f}$) in (4) with the assurance that no pressure-velocity decoupling may occur.

In the constitutive equation it is also necessary to compute the stresses at cell faces from the stresses at nodal values and there is a stress-velocity coupling problem, akin to the pressure-velocity coupling. If a linear interpolation of nodal values of stress is used to compute face values, a possible lack of connectivity between the stress and velocity fields may result. Oliveira et al (1997) devised the following method: starting with equation (8), all terms are arithmetic-averaged to a particular cell-face f, except those multiplying velocity differences accross the faces (l=f in Eq. 9), which are evaluated directly via

$$\overline{a_P^{\tau}}\tilde{\tau}_{ij}^f = \overline{H(\tau_{ij})} + \overline{b_{fj}}[\Delta u_i]_f^f + \overline{b_{fi}}[\Delta u_j]_f^f + \left(\overline{\sum_{l\neq f}^2 b_{lj}[\Delta u_i]_l^P + \sum_{l\neq f}^2 b_{li}[\Delta u_j]_l^P} \right) + \overline{S^{\tau_{ij}}} \tag{10}$$

Here $S^{\tau_{ij}}$ contains the source terms not explicitly written and $H(\tau_{ij})$ and the b- coefficients are

$$H(\tau_{ij}) \equiv \sum_F a_F^{\tau}(\tau_{ij})_F \tag{11-a}$$

$$b_{li} = \eta B_{li} + \lambda \sum_k^3 B_{lk}\tau_{ik} \tag{11-b}$$

The velocity differences in equation (10) are evaluated according to the adopted notation, with cell-centered ($[\Delta u]^P$) and face-centered ($[\Delta u]^f$) values carefully separated. See the original reference for further details.

3.1-The Pressure-Velocity Algorithm Extended to the Stress

The calculation of pressure is carried out indirectly, since the momentum equation, where pressure is explicitly present, is used for computing the velocity vector. Here we adopt

the pressure-velocity correction technique of Patankar and Spalding (1972), known as SIMPLE. Two new steps are introduced in the SIMPLE-like algorithm to account for the stress equation, as follows:

- The stress field results from the solution of the six implicit constitutive equations, just before the three momentum equation are handled for the first time. The stress components are sequentially obtained from their implicit constitutive equations (from 8):

$$a_{\mathrm{P}}^{\tau}\tau_{ij-\mathrm{P}}^{*} = \sum_{\mathrm{F}} a_{\mathrm{F}}^{\tau}\left(\tau_{ij}^{*}\right)_{\mathrm{F}} + S_{\tau_{ij}} \qquad (12)$$

where the coefficients and source term are obtained from the previous time-level values.

- Then, the momentum equations are solved implicitly for each velocity component, with the stresses from (12) being included into the source term. The very important step here is to base the cell face-stress components in the divergence term (7-c) on the interpolation practice defined by equation (10).

The pressure gradient term is based on previous time-level values and the stress-related source term is based on newly obtained cell-face stress $\tilde{\tau}_{ij}^{*f}$, which require the central coefficient of the stress equation (a_{P}^{τ}). This explains the need for solving the stress equation before the momentum equation.

Corrected velocity components do not generally satisfy the continuity equation. The third step of the algorithm involves an update of the corrected velocities so that a new velocity will satisfy continuity as in the pressure-velocity correction procedure of Patankar and Spalding (1972).

3.2- Boundary Conditions

At the inlet the velocity vector is given as a profile. The stress field depends on the velocity field, but since a general constitutive equation is implicit in the stress it becomes numerically difficult to express the stresses at inlet in an explicit way. An alternative and sensible approach adopted in the present work was to anticipate the inlet further and to assume a fully developed flow condition in order to get an explicit stress field. The flow is then allowed to develop and leads to the correct stress field further downstream, in the region of interest.

The outlet is located far from the region of interest and the flow is allowed to redevelop, so that it is safe to assume zero gradients of all variables (velocities, stresses and pressure) along the main flow direction. It is also necessary to adjust the velocities at these boundary faces so that overall mass conservation is satisfied.

Accross a symmetry plane convective and diffusive fluxes of all quantities must vanish. Fictitious boundary cells were created and the reflexion laws applied to define the boundary conditions at their cell-faces f, as presented in Oliveira et al (1997).

For solid walls the no-slip condition applies for the velocity. The wall pressure is linearly extrapolated from the two nearest neighbour cells, the practice used in classical Newtonian CFD. The stresses at a wall situated at a general cell face f are given by the equations (13), derived from the fluid model.

$$J\tau_{ij} = \eta\left[\beta_{fj}\frac{\partial u_i}{\partial \xi_f} + \beta_{fi}\frac{\partial u_j}{\partial \xi_f}\right] + \lambda_f\left[\left(\beta_{fk}\tau_{kj}\right)\frac{\partial u_i}{\partial \xi_f} + \left(\beta_{fk}\tau_{ki}\right)\frac{\partial u_j}{\partial \xi_f}\right] - \frac{2}{3}\eta_f\beta_{fk}\frac{\partial u_k}{\partial \xi_f}\delta_{ij} \qquad (13)$$

The convective terms are zero and the velocity differences $\partial u_i/\partial \xi_f$ are to be written for the case of a solid wall. Application of this equation to an orthogonal geometry such as this yields simpler explicit expressions for the stress components.

4. FLOW GEOMETRY AND COMPUTATIONAL MESH

The 4:1 planar contraction used here, also considered by Sato and Richardson (1994), is sketched in figure 2. The figure defines the coordinate system and some of the nomenclature here used.

The calculation domain spans from -100 mm to +100 mm in the longitudinal direction, corresponding to ±10 downstream channel half-heights (H_2), and the inlet half height is 40 mm. The upstream size is sufficient for the inlet flow to be unaffected by the contraction, whereas the downstream length is sufficient for the flow at the contraction plane to be unaffected by outlet conditions and for the flow to become almost fully-developed for the present Reynolds numbers. The density of the fluid was 1000 kg/m^3, the dynamic viscometric viscosity μ= 0.5 Pas and the time constant λ took values from 0 to 200 s. The Reynolds and Deborah number are based on the downstream pipe and were calculated as follows

$$\mathrm{Re} = \frac{\rho U_2 H_2}{\mu} \tag{14}$$

$$De = \frac{\lambda U_2}{H_2} \tag{15}$$

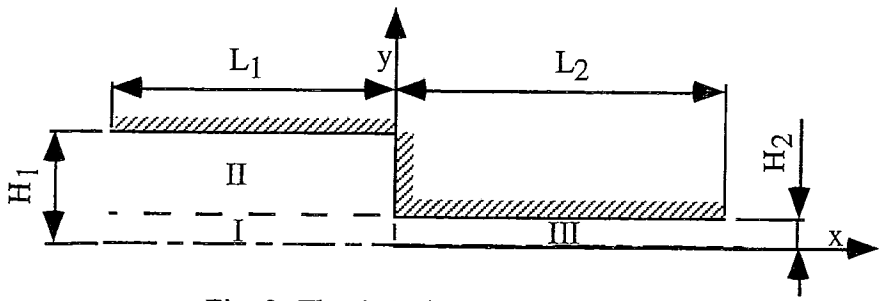

Fig. 2- The 4: 1 planar contraction

Converged solutions were obtained for Reynolds numbers of 0.01 and 10 and Deborah numbers from 0 to 10.0, clearly in excess of the maximum values obtained by Yoo and Na (1991), but only the results pertaining to De= 0.0 and 2.0 are reported here in detail. The Deborah number defined here corresponds to the Weissenberg number used by Sato and Richardson (1994), therefore our tests are directly comparable to theirs at numerically identical values of the elastic parameter. However, whereas Sato and Richardson's calculations pertain to an Oldroyd B fluid, with a ratio of retardation to relaxation times of 0.11, the present calculations are for an UCM fluid. For the low Reynolds number case (Re= 0.01) converged solutions were obtained with UDS up to De= 10 and LUDS was used for De= 0. For the higher Reynolds number (Re= 10) LUDS was also used for the Newtonian case.

The two-dimensional geometry was divided into three blocks used to define computational meshes (see Fig. 2), with block I having 60 x 20 cells, block II 60 x 40 and block III 60 x 20 in the finer mesh. The cells were made smaller as the contraction plane and the reentrant corner were approached using appropriate geometrical factors, so that at the corner the minimum cell size was of $\delta_{x,min}$= 0.30 mm and $\delta_{y,min}$ = 0.30 mm (non-dimensionally, δ_{xmin}/H_2= 0.03). The geometrical factors in the finer mesh were (f_x= 0.95367, f_y= 0.95), (f_x= 0.95367, f_y= 1.0436) and (f_x= 1.04858, f_y= 0.95) for blocks I, II and III, respectively.

5. RESULTS AND DISCUSSION

Figure 3 shows streamline plots pertaining to low (Re= 0.01) and high (Re= 10) Reynolds number flows with inelastic and elastic (De= 2) fluids.

In the absence of fluid elasticity, and for very small Reynolds numbers, there is a weak recirculation in the upstream side of the sudden contraction, attached to the salient corner. Convection reduces the size of the eddy, which becomes localised to the corner itself. The appearance of a lip vortex merged with the primary vortex is noticed in figure 3-b) and is attributed to the fluid elasticity. Even at higher Reynolds numbers, where the recirculation zones are smaller, a very small lip vortex is predicted.

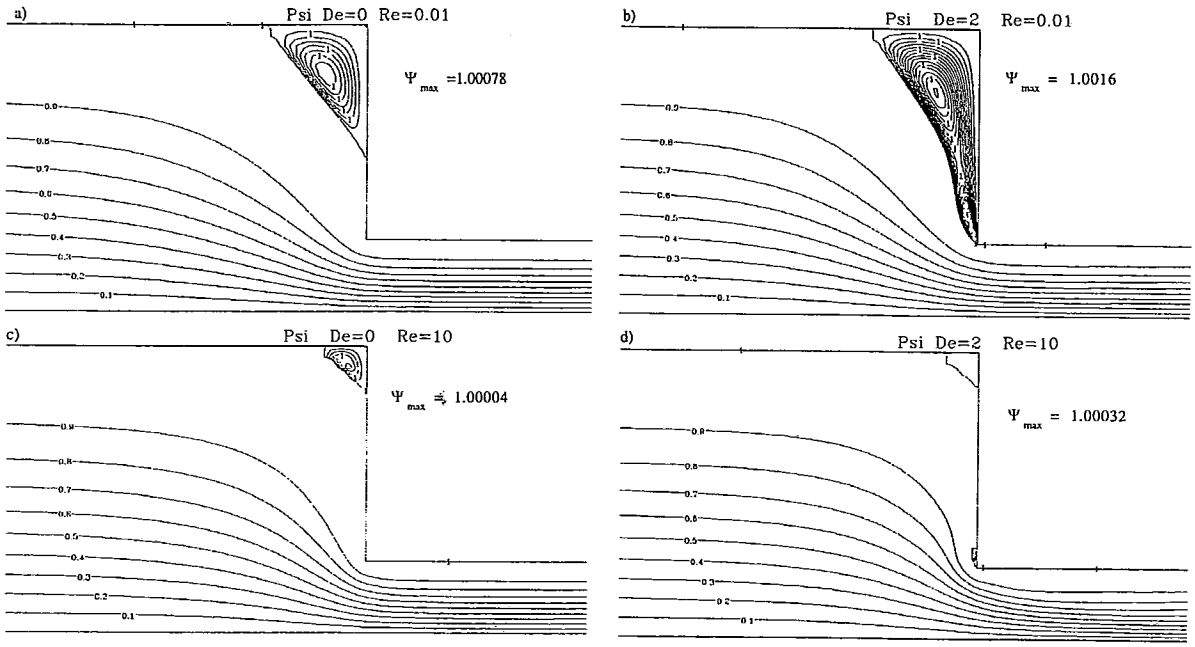

Fig. 3- Streamlines (Psi) in the vicinity of the sudden contraction for various flow conditions.

Lip vortices associated with fluid elasticity have been reported in the past both in many experimental works (Evans and Walters, 1988) as well as numerically (Sato and Richardson, 1994; Purnode and Crochet, 1996; Yoo and Na, 1991). These authors observed a very similar behaviour to that reported here at low and high Reynolds numbers, although the numerical values of the non-dimensional parameters were not the same, because they depend on the constitutive relation which were different from this work. The middle authors used the FENE-P model adjusted to the rheology of 1%, 0.5% and 0.25% aqueous polyacrilamide solutions, whereas the latter used the Oldroyd-B model, a more similar equation and as a consequence their results are closer to ours in that they show a lip vortex at De= 0.3 and Re= 0. This is, however, the first time when final steady-state lip vortex are predicted with UCM (Sato and Richardson refers to such structures during a time-developing period)

Vortex growth is usually attributed to elasticity of elongational nature rather than to shear elasticity (White and Baird, 1988) and that explains the small effect of the Deborah number upon the recirculation length when using models which are not good at simulating a high elongational viscosity over a large range of strain rates as is the case of the Oldroyd-B and UCM models.

In figure 4 the predicted recirculation length is compared with data from the literature pertaining to calculations as well as experiments. Comparison with experiments must be done carefully because real fluids do not follow the simple UCM constitutive equation.

Nevertheless the current predictions of eddy length are in good agreement with those of Sato and Richardson: at very low Reynolds numbers the recirculation length is either approximately constant or slightly decreasing with De, for Deborah numbers lower than 2 and faster for higher elasticity, a feature not detected by Sato and Richardson whose maximum Deborah number was 2. As the Reynolds number is increased the effect of the fluid elasticity is reversed, and our predictions again compare favourably with those in the literature: the calculations of Sato and Richardson for Re= 1 are intermediate between the current predictions for Re= 0.01 and Re= 10.

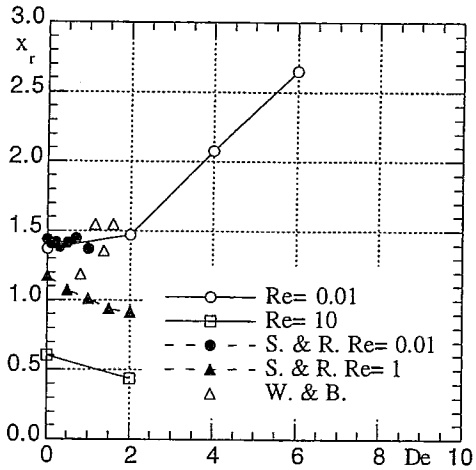

Fig. 4- Comparison between the predicted and literature data on the corner vortex length (S. & R.- Sato and Richardson, 1994; W. & B.- White and Baird, 1988).

The stress field for the flow cases in figure 3a)-d) are presented in figures 5, 6 and 7: contours of the normalised stresses T_{11}, T_{22} and T_{12}, correspond to the non-dimensionalised normal stresses τ_{xx}, τ_{yy} and shear stress τ_{xy}, respectively, where the normalisation was performed with $\mu\, U_2/H_2$.

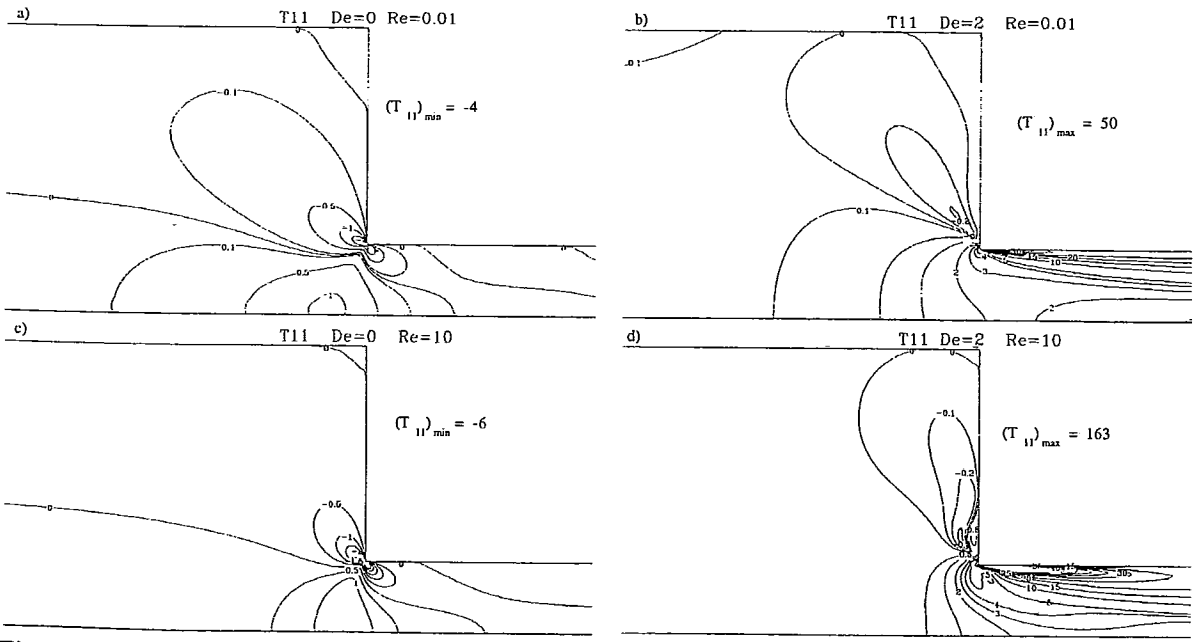

Fig. 5- Contours of the normalised axial normal stress (T_{11}) in the vicinity of the sudden contraction.

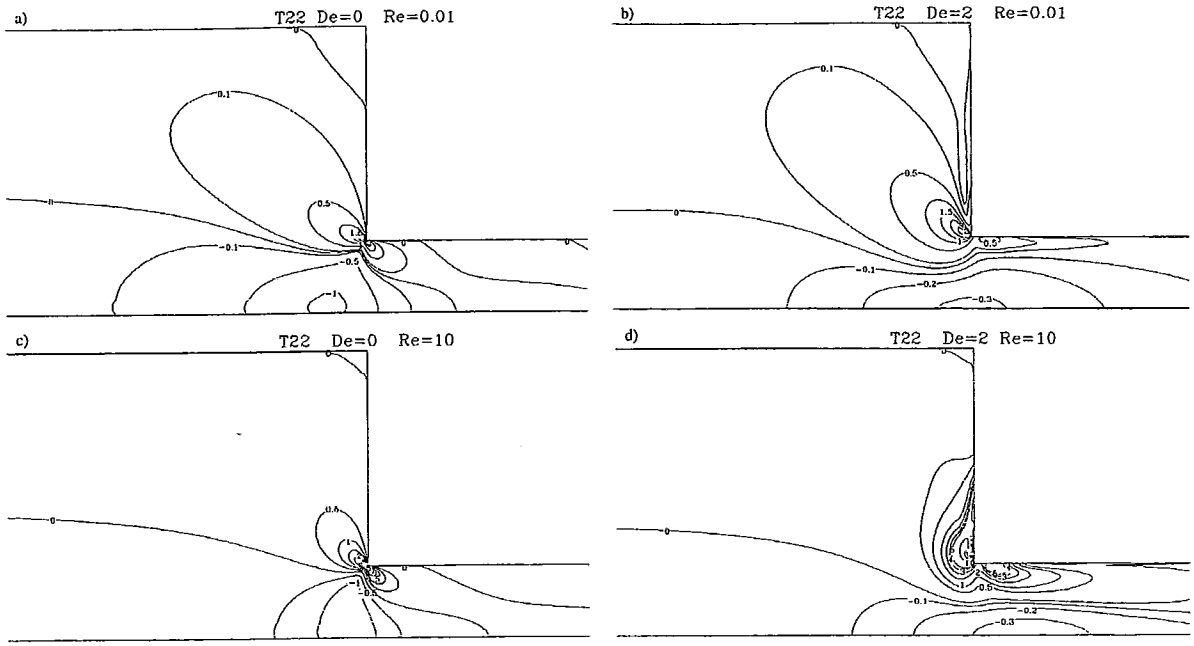

Fig. 6- Contours of the normalised transversal normal stress (T_{22}) in the vicinity of the sudden contraction.

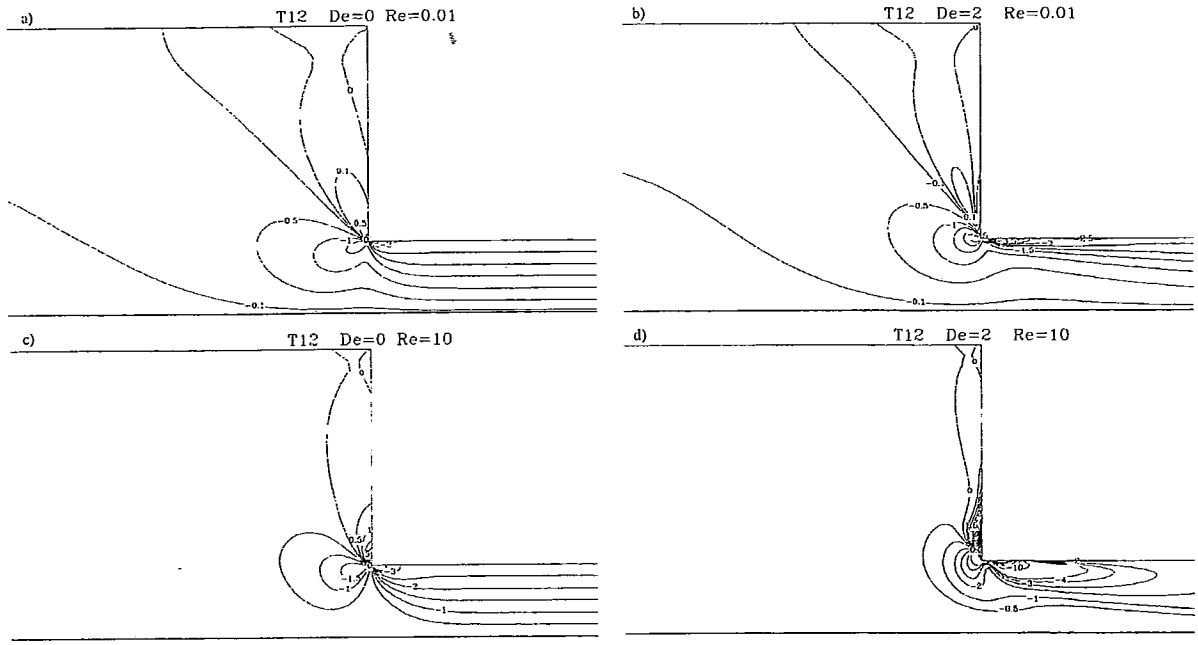

Fig. 7- Contours of the normalised shear stress (T_{12}) in the vicinity of the sudden contraction.

For a Newtonian flow, and by virtue of mass conservation, the transversal normal stress (T_{22}) is symmetric to the axial normal stress (T_{11}) , regardless of the Reynolds number (compare Figs. 5a and 5c with Figs 6a and 6c, respectively). Changes to this behaviour are proper of elasticity, especially when coupled with inertia. At low Reynolds numbers the elastic flow upstream of the contraction still exhibits a contour pattern for both T_{11} and T_{22} which bears resemblance to that of inelastic fluids, but as the re-entrant corner is approached the similarity ends. Very high stresses develop, especially so for T_{11}, and they persist along the wall of the downstream channel due to a convection effect on the stress equation, defining high positive values of the first normal stress difference N_1. It is also clear that there are two regions of maximum stresses: the region of the lip vortex in the contraction side wall and in the

downstream channel wall immediately after the re-entrant corner. It is precisely this strong increase in the axial normal stress which is responsible for the larger pressure drop in the flow through sudden contractions of elastic fluids.

These two regions of high stresses are also observed in the shear component (figure 7) although the difference between the maxima for Newtonian and elastic fluids are not so intense as with the normal axial stress but where, still, the downstream contraction region is very different for De= 2 compared with De= 0 (Newtonian). Note, however, that the normal stress difference increase is considerably less than was observed in the experiments of White and Baird (1988) with LDPE and similar to that of polystyrene (see figure 8). Whereas polystyrene was found to exhibit no major eddy increase with the Deborah number, as in this work, the LDPE showed the expected increase in x_r with De and simultaneously a larger elongational viscosity than polystyrene.

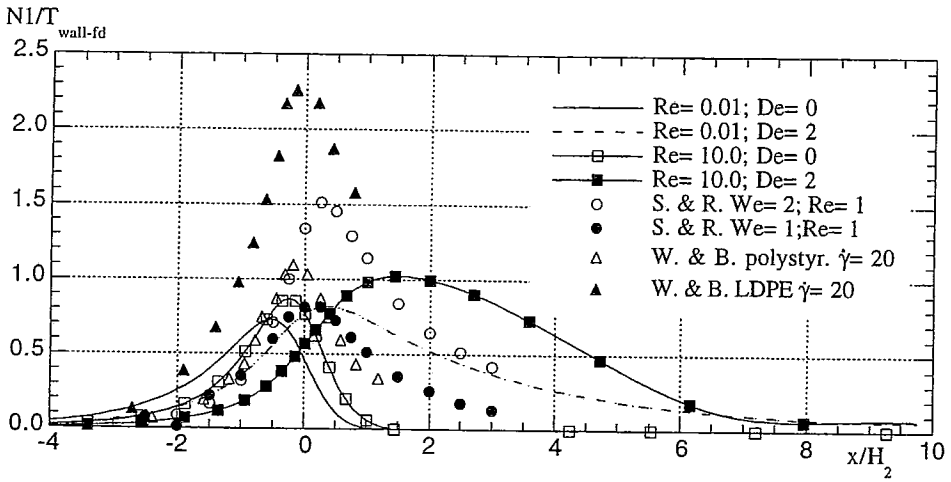

Fig. 8- Comparison between experimental and calculated longitudinal profiles of N_1/τ_{wall}. (S. & R.- Sato and Richardson, 1994; W. & B.- White and Baird, 1988)

6. CONCLUSIONS

A finite-volume based numerical algorithm has been developed for the calculation of viscoelastic fluids in a general non-orthogonal colocated grid. All terms of the various equations were kept and the discretization and interpolation techniques were either first or second order accurate, with the first type sometimes required to ensure convergence. To ensure pressure- velocity- stress coupling a new interpolation technique has been presented.

Calculations in a 4:1 planar contraction were carried out for one-mode Upper Convected Maxwell models and convergence was attained for various Reynolds numbers and for Deborah numbers up to 10. Here we focus on the cases De= 0 and De= 2.

The predictions were in agreement with observation and numerical data from the literature. The length of the primary recirculation bubble was seen to increase with elasticity at very low Reynolds numbers, as expected, but to decrease with increased inertia.

In the contraction, high values of the stress developed especially for the axial normal stress, thus leading to higher pressure drop in comparison to the Newtonian flow at the same Reynolds number.

Thus, the programme seems fit to deal with more complex geometries and fluids, a step to be undertaken in the near future.

ACKNOWLEDGEMENTS

The authors would like to acknowledge the financial support of project PBIC/P/QUI/1980/95 of JNICT- Junta Nacional de Investigação Científica e Tecnológica.

REFERENCES

Baloch, A., Townsend, P. and Webster, M. F. 1994 Extensional Effects in Flows Through Contractions With Abrupt or Rounded Corners, *J. Non-Newt. Fluid Mech.*, 54, 285-302.

Boger, D. V. and Walters, K. 1993. *Rheological Phenomena in Focus*, Rheology Series Volume 4, Elsevier, Amsterdam.

Boger, D. V. and Hur, D. U. and Binnington, R. J. 1987. Further Observations of Elastic Effects in Tubular Entry Flows. *J. Non-Newt. Fluid Mech.*, 20, 31-49.

Boger, D. V and Ramamurthy, A. M. 1970. Experimental measurements of loss coefficients in the entrance region of a pipe for viscous power law and viscoelastic fluids. *A. I. Ch. E. J.*, 16, 1088 - 1091.

Crochet, M. J. and Pilate, G. 1976. Plane flow of a fluid of second grade through contractions. *J. Non-Newt. Fluid Mech.*, 1, 247- 258.

Evans, R. E. and Walters, K. 1988. Flow characteristics associated with abrupt changes in geometry in the case of highly elastic liquids. *J. Non-Newt. Fluid Mech.*, 20, 11-29.

Ferziger, J. H. and Peric, M. 1996. *Computational Methods for Fluid Dynamics.* Springer Verlag, Berlin.

Hu, H. H. and Joseph, D. D. 1990. Numerical simulation of viscoelastic flow past a cylinder. *J. Non-Newt. Fluid Mech.*, 37, 347-377.

Lawler, J. V., Muller, S. J., Brown, R. A. and Armstrong, R. C. 1986. Laser Doppler velocimetry measurements of velocity fields and transitions in viscoelastic fluids. *J. Non-Newt. Fluid Mech.*, 20, 51-92.

Oliveira, P. J. , Pinho, F. T. and Pinto, G. A. 1997. A Finite Volume Colocated-Mesh Method for the Prediction of Non-Newtonian Fluid Flow. Submitted to *J. Non-Newt. Fluid Mech.*

Patankar, S. V. and Spalding, D. B. 1972. A calculation procedure for heat, masss and momentum transfer in three-dimensional parabolic flows. Int. J. Heat and Mass Transfer, 15, 1787.

Perera, M. G. N. and Walters, K. 1977. Long range memory effects involving abrupt changes in geometry. Part II: The expansion/ contraction/ expansion. *J. Non- Newt. Fluid Mech.*, 2, 191-204.

Purnode, B. and Crochet, M. 1996. Flows of polymer solutions through contractions. Part 1: flows of polyacrylamide solutions through planar contractions. *J. Non-Newt. Fluid Mech.*, 65, 269-289.

Quinzani, L. M., Armstrong, R. C. and Brown, R. A. 1994. Birefringence and laser-Doppler velocimetry studies of viscoelastic flow through a planar contraction. *J. Non-Newt. Fluid Mech.*, 52, 1-36.

Rajagopalan, D., Armstrong, R. C. and Brown, R. A. 1990. Finite element methods for calculations of steay viscoelastic flow using constitutive equations with a Newtonian viscosity. *J. Non-Newt. Fluid Mech.*, 36, 159- 192.

Rhie, C. M. and Chow, W. L. 1982. A numerical study of the turbulent flow past an isolated airfoil with trailing adge separation. *AIAA*, 82, 998.

Sasmal, G. P. 1995. A finite volume approach for calculation of viscoelastic flow through an abrupt axisymmetric contraction. *J. Non-Newt. Fluid Mech.*, 56, 15-47.

Sato, T. and Richardson, S. 1994. Explicit numerical simulation of time-dependent viscoelastic flow problems by a finite element/ finite volume method. *J. Non-Newt. Fluid Mech.*, 51, 249-275.

Walters, K. and Webster, M. F. 1982. On dominating elastico-viscous response in some complex flows. *Phil. Trans. Royal Soc. London*, 308, 199-218.

Webster, M. F. 1986. A technique to solve incompressible non-newtonian flow problems. *J. Non-Newt. Fluid Mech.*, 20, 227-240.

White, S. A. and Baird, D. G. 1988. Flow visualization and birefringence studies on planar entry flow behavior of polymer melts. *J. Non-Newt. Fluid Mech.*, 29, 245-267.

Yoo, J. Y. and Na, Y. 1991. A numerical study of the planar contraction flow of viscoelastic fluids using the SIMPLER algorithm. *J. Non-Newt. Fluid Mech.*, 39, 89-106.